Efficient Protein-Facilitated Splicing of the Yeast Mitochondrial bI5 Intron[†]

Kevin M. Weeks and Thomas R. Cech*

Department of Chemistry and Biochemistry, Howard Hughes Medical Institute, University of Colorado, Boulder, Colorado 80309-0215

Received February 1, 1995; Revised Manuscript Received April 4, 1995[⊗]

ABSTRACT: The splicing factor CBP2 is required to excise the yeast mitochondrial group I intron bI5 *in vivo* and at low magnesium ion concentrations *in vitro*. CBP2 binding is strengthened 20-fold by increasing Mg^{2+} concentrations from 5 to 40 mM, implying the protein binds, in part, to the same structure as that stabilized by the cation. The same transition is also observed as a cooperative increase in the rate of self-processing between 5 and 40 mM Mg^{2+}, providing strong evidence for an RNA folding transition promoted by either Mg^{2+} or CBP2. The first step of splicing, guanosine addition at the 5′ splice site, is rate limiting for exon ligation. At low (5 mM) magnesium ion, reaction (measured as k_{cat}/K_m or k_{cat}) is accelerated 3 orders of magnitude by saturating CBP2. At near-saturating Mg^{2+} (40 mM), acceleration is 8- and 30-fold, for k_{cat} and k_{cat}/K_m, respectively, so high magnesium ion concentrations fail to compensate completely for protein facilitation. Thus, self-splicing proceeds via two additional transitions as compared with reaction of the bI5·CBP2 complex, only the first of which is efficiently promoted by the cation. Guanosine 5′-monophosphate binds ($K_d \approx 0.3$ mM) with the same affinity to bI5 and the bI5−protein complex, supporting independent binding of the nucleophile and CBP2. Substitution of a phosphorothioate at the 5′ splice site and pH profiles provide evidence that k_{cat} is limited by chemistry at low pH and by a conformational step at high pH. Because binding by either Mg^{2+} or CBP2 increases the rate of chemistry more than the rate of the conformational step, in the physiological pH range (7−7.6) the protein-facilitated reaction is limited by a conformation step while self-splicing reaction is limited by chemistry. We conclude that CBP2 makes manifold contributions to bI5 splicing: binding compensates for at least two structural defects and accelerates the rate of the chemistry.

Self-splicing by group I introns is mediated by a conserved secondary and tertiary folding of the RNA and requires magnesium or manganese ion. Splicing occurs via sequential transesterification reactions, initiated by attack of an exogenous guanosine nucleophile (Cech, 1990). Although many group I introns have been shown to self-splice *in vitro*, other closely related introns that appear to be able to form similar secondary (and presumably tertiary) structures do not self-process well. Self-processing *in vitro* suffers from several common defects. In many cases, unphysiologically high magnesium ion concentrations are required for optimal activity (Garriga & Lambowitz, 1984; van der Horst & Tabak, 1985; Hicke et al., 1989; Jaeger et al., 1991). Additionally, reaction kinetics are complex, with only a fraction, often much less than 50%, reacting in an initial fast transition (Bass & Cech, 1984; van der Horst & Tabak, 1985). Even the archetypal *Tetrahymena* ribozyme, which readily undergoes self-processing under physiological conditions *in vitro*, does so 20 times more slowly than the rate estimated *in vivo* (Brehm & Cech, 1983). There is accumulating evidence that many of these defects may be remedied by proteins *in vivo* (Cech, 1990; Lambowitz & Perlman, 1990; Guo & Lambowitz, 1992; Coetzee et al., 1994).

Biogenesis of the *Saccharomyces cerevisiae* mitochondrial cytochrome *b* messenger RNA requires removal of several introns, including the terminal group I intron, bI5. The nuclear-encoded CBP2 protein is required for excision of the A-U rich bI5 intron from the pre-mRNA (McGraw & Tzagoloff, 1983). In the presence of CBP2, the intron correctly splices at physiological concentrations of magnesium ion (5 mM) *in vitro*, while optimal splicing in the absence of protein requires ~50 mM Mg^{2+} and is undetectable at 5 mM magnesium (Gampel & Tzagoloff, 1987; Partono & Lewin, 1988, 1991; Gampel et al., 1989; Gampel & Cech, 1991). The observation of self-splicing at high magnesium ion concentrations and the sensitivity of the protein-dependent reaction to mutations in the guanosine-binding site (Gampel & Cech, 1991; Michel et al., 1989) emphasize that the RNA provides key catalytic elements under all conditions.

Because catalytic structures both in the presence and absence of protein are reported directly as splicing activity, the bI5−CBP2 system provides a convenient and robust model for protein−RNA interactions and for the contributions made by splicing factors in RNA processing. Analogous protein-facilitated but intrinsically RNA-catalyzed reactions may be common elements of complex RNA−protein machines like the ribosome and spliceosome [for example, see Noller et al. (1992)]. Here, we develop thermodynamic and kinetic frameworks to compare protein-facilitated and protein-independent splicing by bI5.

EXPERIMENTAL PROCEDURES

Expression and Purification of CBP2. CBP2 was expressed as a C-terminal $(His)_6$ fusion. The cDNA for CBP2 was obtained from plasmid pG36/T5 (McGraw & Tzagoloff, 1983). PCR was used to (1) add a recognition site for *Xma*I

[†] This work is supported by a fellowship to K.M.W. from the Jane Coffin Childs Memorial Fund for Medical Research. T.R.C. is an investigator of the Howard Hughes Medical Institute and an American Cancer Society Professor.

* Author to whom correspondence should be addressed.

[⊗] Abstract published in *Advance ACS Abstracts,* May 15, 1995.

0006-2960/95/0434-7728$09.00/0

and a ribosome binding site 5′ to the gene and (2) add five extra histidine codons, a new stop codon, and a site for *Spe*I 3′ to CBP2 coding sequences. After digestion with the appropriate enzymes, the PCR fragment was cloned into plasmid pT5T (Squires et al., 1988), which contains sequences required for T7 RNA polymerase-driven overexpression, to create plasmid pCBP2H6. Coding and regulatory sequences were confirmed by dideoxy sequencing. CBP2 was expressed from pCBP2H6 in *Escherichia coli* strain BL21(DE3)plysS at 22 °C. Cells were grown in 2×YT media supplemented with 5 mM glucose, 20 mM potassium phosphate (pH 7.8), 12.5 μg/mL tetracycline, and 17 μg/mL chloramphenicol. CBP2 expression was induced at OD_{600} = 0.8 by addition of IPTG to 1 mM, and growth was continued an additional 6 h. Pelleted cells were resuspended in 10 mL of ice-cold column buffer [CB: 50 mM hepes (pH 7.6), 700 mM NaCl, 10% glycerol, 5 mM 2-mercaptoethanol, 0.02% NaN_3] supplemented with 1 mM IPTG and lysed by sonication. Subsequent purification steps were performed at 4 °C. Lysates were cleared by centrifugation (30 min at 38 000 rpm in a Beckman 70Ti rotor) and subsequently stirred with 4 mL of Ni^{2+}−nitrilotriacetic acid−agarose resin (Qiagen) for 1 h. After addition of imidizole (pH 7.6) to 1 mM, a 1.6 cm diameter column was poured from the lysate−resin mixture. The column was then washed with 40 mL (10 column volumes) of CB followed by 25 mL each of CB plus (1) 20 mM imidizole, (2) 80 mM imidizole, and (3) 200 mM imidizole. CBP2-containing fractions (2 mL each) eluted in the 80 mM imidizole wash and were dialyzed exhaustively (15 kDa cutoff) against 20 mM Hepes (pH 7.6) 200 mM NaCl, 0.1 mM EDTA, 40% glycerol, and 2 mM DTT and subsequently stored in this buffer at −20 °C. No loss of activity during storage was detected over a period of 2 years.

The N-terminal sequence of the recombinant protein [see McGraw and Tzagoloff (1983)] was confirmed by amino acid sequencing (Clive Slaughter, University of Texas Southwestern Medical Center) and found to include the initiator amino acid fMet. The purity of recombinant CBP2 was estimated to be ≥95% from overloaded Coomasie blue stained protein gels. The concentration of CBP2 was determined (1) by using a calculated extinction coefficient of 80 300 M^{-1} cm^{-1} at 280 nm (Gill & von Hippel, 1989) or (2) from an excess RNA stoichiometric binding assay (see below). Concentrations determined from the two methods agreed within 30%.

Template Construction. The "wild-type" bI5 precursor contains 180 nt 5′ of the intron, the 738 nt bI5 intron, and a 48 nt 3′ exon. Oligonucleotide-directed phagemid mutagenesis (Kunkel, 1985) of pTZ18U/bI5 (Gampel & Cech, 1991) was used to (1) delete nt 10-213 in L1 [this deletion maintains P10, which base pairs with the 3′ exon and whose integrity is required for efficient exon ligation (Partono & Lewin, 1990); see Figure 2], (2) replace nt 387−410 in L6 with a C(UUCG)G tetraloop, and (3) replace nt 502−653 in L8 with the sequence AGAUCU [this last deletion was described by Gampel and Cech (1991)]. These deletions remove a net 207, 17, and 146 nt, respectively, and yield a simplified intron of 368 nt. Mutations were confirmed by sequencing. Plasmids were linearized with *Xba*I to generate templates for runoff transcription by T7 RNA polymerase. Templates encoding deletions in the 5′ exon were obtained from large scale (1−2 mL) PCR reactions; the 5′ primer included sequences required to generate a T7 promoter. Most experiments were performed with bI5−5R RNA which includes a 35 nt 5′ exon, 368 nt intron, and 55 nt 3′ exon to yield a 458 nt precursor (the complete renumbered sequence of the 5R intron is given in Figure 2).

RNA Precursors. Transcription reactions (0.5−3 mL) were incubated at 37 °C for 3−6 h and contained 80 mM Hepes (pH 7.6), 40 mM DTT, 2 mM spermidine, 20 mM $MgCl_2$, 2.5 mM each nucleoside triphosphate, 0.01% triton X-100, 20 μg of template/mL reaction, and 5000 units/mL phage T7 RNA polymerase. Following purification in 4% acrylamide gels, bands corresponding to full length precursors were excised and electroeluted from gel using an Elutrap apparatus (Schleicher and Schuell), precipitated with ethanol, resuspended in 10 mM Tris (pH 7.5) and 1 mM EDTA, and stored at −20 °C. RNA concentrations were calculated assuming an extinction coefficient of 8600 M^{-1} cm^{-1} $residue^{-1}$ at 260 nm. 5′-^{32}P-labeled RNAs were generated by treatment with calf intestinal phosphatase followed by reaction with polynucleotide kinase and [γ-^{32}P]ATP, repurified by gel electrophoresis, excised from the gel, eluted overnight into 0.5 M sodium acetate (pH 6) and 1 mM EDTA at 4 °C, precipitated with ethanol, and resuspended in 1 mM Tris (pH 7.6) and 0.1 mM EDTA.

Velocity Sedimentation. A 3.3 mL 10−50% glycerol gradient in 20 mM hepes (pH 7.6), 200 mM NaCl, 0.1 mM EDTA, and 2 mM DTT was poured using a manual gradient mixer. CBP2 (at 2 μM in 1× gradient buffer containing 3% glycerol) plus size markers were placed at the top of the gradient. Samples were centrifuged for 15 h at 50 000 rpm in a Beckman SW55Ti rotor at 4 °C. Fractions (250 μL) were removed from the bottom of the centrifuge tube, and the contents of each fraction were analyzed by electrophoresis (Phast Gel System, Pharmacia). The final concentration of CBP2 after dilution in the gradient was estimated to be 300−500 nM. Molecular weight standards were 29, 150, 200, and 443 kDa.

Reaction Conditions. Precursor RNAs were heated to 90 °C for 1 min in 1 mM Tris (pH 7.5) and 0.1 mM EDTA and then placed on ice to eliminate aggregates that form during storage. Precursors were subsequently incubated at 35 °C for 30 min in 1× reaction buffer [50 mM Hepes (pH 7.6), 50 mM KCl, and 5−80 mM $MgCl_2$] to permit refolding. All binding and splicing reactions were performed at 35 °C in reaction buffer containing $^1/_{10}$ volume of protein dilution buffer [20 mM Hepes (pH 7.6), 200 mM NaCl, 0.1 mM EDTA, 2 mM DTT, 1 mg/mL BSA, 40% glycerol; containing CBP2, where appropriate]. Thus the final reaction conditions were 52 mM Hepes (pH 7.6), 50 mM KCl, 20 mM NaCl, $MgCl_2$ (defined for each experiment in the figure and table legends), 0.2 mM DTT, 100 μg/mL BSA, and 4% glycerol. pH-dependence experiments were performed in the same solution except the following buffers were substituted for Hepes in the reaction buffer: pH 5−6, Mes; pH 6.5, Pipes; pH 8−8.5, Taps; pH 9, Ches. After addition of CBP2, reactions were incubated an additional 10−30 min to ensure complete protein binding.

Binding Assays. Equilibrium dissociation constants were determined by either native gel mobility shift assays or by filter binding. The two methods gave indistinguishable results. In practice, after demonstrating that the RNA−protein complex was well behaved as visualized in the mobility shift assay, dissociation constants were determined using the faster and simpler filter binding assay.

For the mobility shift assay, reactions were loaded onto a running 5% (29:1 bis/acrylamide) gel; both the gel and the running buffer contained 50 mM Tris-borate and 5 mM $MgCl_2$. Electrophoresis was performed for 2 h at 20 V/cm at 20−25 °C.

Filter binding was performed using a simplification of the dual filter method of Wong and Lohman (1993) which employs a 96-well dot blot apparatus. Pure nitrocellulose and Hybond N+ membranes (Amersham) were equilibrated against 50 mM Hepes (pH 7.6) and 50 mM KCl for 30 min prior to assembly of the apparatus. Wells were washed with 50 μL of 1× reaction buffer after which 8−12 reactions (20 μL) were filtered. Wells were subsequently washed with 50 μL of ice-cold 1× reaction buffer.

Equilibrium dissociation constants were determined for either method by quantifying the fraction RNA bound (θ) with a PhosphorImager (Molecular Dynamics) and performing a nonlinear least-squares fit as a function of free CBP2 concentration,

$$\theta = \epsilon \frac{[\text{CBP2}]}{[\text{CBP2}] + K_d}$$

where ϵ is the observed maximum fraction bound (typically ≥0.9 for mobility shift assays and 0.6−0.8 for filter binding assays). RNA concentrations were at least 10-fold below the apparent K_d's. Control experiments were performed in which binding reactions at 5, 10, and 40 mM $MgCl_2$ were incubated 20, 60, and 150 min before filtering. Measured dissociation constants at all magnesium ion concentrations were independent of incubation time, confirming that equilibrium had been attained; filter binding ϵ's decreased from 80 to 60% as the [$MgCl_2$] increased from 5 to 40 mM.

Kinetics. Self-splicing reactions are by definition single turnover; protein- facilitated reactions were also performed under single-turnover conditions (CBP2 in excess over RNA and present at [CBP2] > K_d). Reactions (20 μL, see above) were initiated by addition of guanosine 5′-monophosphate (pG). Aliquots were removed at specific times, and splicing was quenched by dilution into 2 volumes of stop solution (10 mM Tris-borate, 50 mM EDTA, 80% formamide, 0.2% SDS, and marker dyes). Reactions were analyzed by electrophoresis in 8% acrylamide, 7 M urea gels and quantified using the PhosphorImager. Using 5′-end-labeled precursors, three species are resolved: starting material (sm), ligated exons (le), and 5′ exon (5′e). Fraction starting material was then calculated as sm/(sm + le + 5′e); this division compensates for differences in amount of RNA loaded and for nonspecific background degradation. Endpoints for the initial fast phase were typically 60−80%. The rate of the second phase (~0.0005 min^{-1}) was generally slow enough relative to the fast phase that setting the rate equal to zero did not introduce significant error. Thus, reaction rates were determined by a least-squares two parameter fit to the first-order equation

$$\text{fraction sm} = f_1 e^{-k_{obs}t} + (1 - f_1)$$

where k_{obs} is the observed rate and f_1 is the fraction reacting in the fast phase. k_{obs} for slow reactions was determined using initial rates after normalizing to an assumed endpoint of 70% reacted. The rate of conversion of precursor in the slow phase places a lower limit on measurable rates of ~0.002 min^{-1} for the fast phase. Seven millimolar was generally chosen as the "low" magnesium ion concentration because k_{obs} for the protein-independent reaction is close to this minimum resolvable rate. That CBP2 was saturating was routinely confirmed by doubling the concentration of protein: observed rates typically varied by less than 20%.

Generation of 5′ Splice Site Phosphorothioate-Substituted Precursor. The phosphate at the 5′ splice site was uniquely substituted with an R_p phosphorothioate by regenerating an intact precursor from the following three RNAs: (1) a 21 nt synthetic RNA spanning positions −31 through −11 (negative numbers denote 5′ exon), (2) a 5′-^{32}P-phosphorylated 11 nt synthetic oligonucleotide spanning positions −10 through +1, and (3) a 442 nt RNA generated by GMP-primed transcription beginning with position G^{+2} and extending through the 3′ exon. The three RNAs were annealed to a cDNA template complementary to positions −26 to +19, ligated together using DNA ligase (Moore & Sharp, 1992), and purified by gel electrophoresis. An unsubstituted intron was produced by using a standard oligoribonucleotide made by solid-phase synthesis for oligo (2). The specific R_p phosphorothioate substitution was generated by solid-phase synthesis of an 11-mer containing a mixture of R_p and S_p phosphorothioate diastereomers at position 1 followed by resolution of the two isomers by reverse-phase HPLC (Slim & Gait, 1991). Precursors were constructed from both HPLC-resolved phosphorothioate-containing oligos, one of which was essentially unreactive; this precursor was assigned as containing the S_p isomer [Rajagopal et al. (1989) as discussed by Herschlag et al. (1991) and Zaug et al. (1994)]. The R_p isomer was used for all experiments reported here. Although the ligated wild-type RNA was shorter than the precursor RNA generated entirely via transcription by four nucleotides and a 5′-phosphate, control experiments established that the two precursors exhibited identical kinetics.

RESULTS

Purification and Molecularity of CBP2. Initial attempts to purify recombinant CBP2 from *E. coli* yielded, upon induction, bands resolved by SDS gel electrophoresis corresponding to full length CBP2 and several shorter polypeptides. These shorter polypeptides presumably corresponded to proteolyzed fragments of CBP2. Subsequent chromatography yielded full length protein that was ~80% pure but had low specific activity (data not shown). CBP2 was then expressed as a C-terminal fusion with $(His)_6$. $(His)_6$ binds tightly to a commercially available Ni^{2+}−agarose resin. Because CBP2 naturally terminates in a histidine residue, only five additional histidines were added to the fusion protein. Serendipitously, the stability of the carboxy-terminal $(His)_6$ fusion in *E. coli* was favorably altered as compared with the native recombinant protein. CBP2, ≥95% pure, can be obtained in a single step by affinity chromatography (data not shown).

The size of recombinant CBP2 was estimated by sedimentation through a glycerol gradient (Figure 1). The apparent molecular mass is 55 ± 7 kDa and is in reasonable agreement with the calculated molecular mass of 74 kDa. This good correlation supports assignment of CBP2 as a monomer in solution.

Self-Splicing by a Simplified bI5 Intron: Rate-Limiting First Step. Previous investigations of splicing by bI5 have been severely hampered by the large size of the precursor

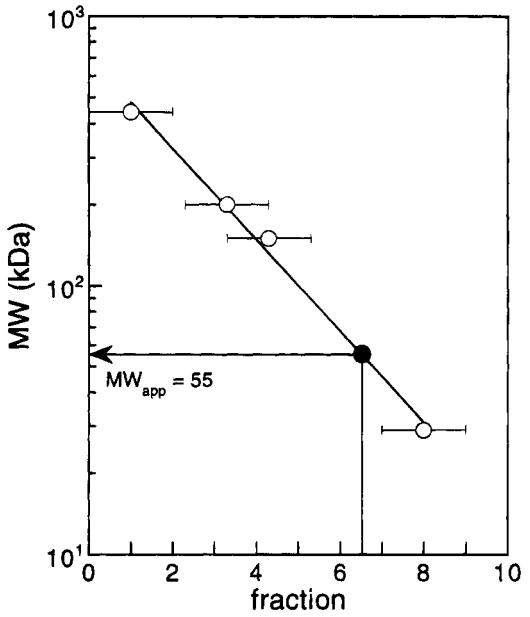

FIGURE 1: Velocity sedimentation analysis of CBP2. Open and solid symbols indicate molecular weight standards and CBP2, respectively.

(~1000 nt). All group I introns share a conserved secondary structure; the native bI5 precursor contains large loops in L1, L6, and L8 that are not found in other group I introns and are located outside the conserved catalytic core believed to form the active site. Moreover, large, relatively unstructured loop regions increase the possibility of misfolding, complicate footprinting and protein binding studies, and, in our hands, exacerbate the ubiquitous problems of nuclease susceptibility and background degradation. Therefore, we deleted the three peripheral loops (L1, L6, and L8) from the 966 nt "native" splicing precursor and eliminated sequences in the 5′ exon to yield a simplified splicing precursor (termed 5R) of 458 nt (Figure 2).

After allowing the native and simplified introns to refold and CBP2 to bind (see Experimental Procedures), protein-facilitated splicing reactions (at 7 mM $MgCl_2$) are initiated by addition of GMP (pG). Using 5′-end-labeled RNA, two products are visualized for both bI5 and 5R RNAs: the ligated exons (le), which is the biologically relevant product, and the free 5′ exon (5′e) (Figure 3A). Comparison of the reaction of native bI5 and 5R reveals that both precursors react with rates of 1.1 ± 0.2 min^{-1} in the initial fast phase, identical within error. However, while only 30% of the native intron reacts in the fast phase, 73% of the simplified intron does, suggesting a greater fraction of the larger native intron is trapped in a slowly reacting conformation(s) (circles in Figure 3B).

Reaction of starting material and formation of ligated exons occur at identical rates within error (Figure 3B and Table 1) during the fast phase. Thus, attack by the guanosine nucleophile or a step preceding cleavage is rate limiting for the overall *on-pathway* reaction as shown by k_I and k_{II} in Scheme 1.

Moreover, for a mechanism of two consecutive irreversible reactions as shown in Scheme 1 for the on-pathway reaction:

$$k(\text{formation of le}) = \frac{k_I k_{II}}{k_I + k_{II}}$$

That k(formation of le) $\approx k_I$ requires $k_{II} \gg k_I$. For example, if $k_I = k_{II}$ then k(formation of le) would be $k_I/2$.

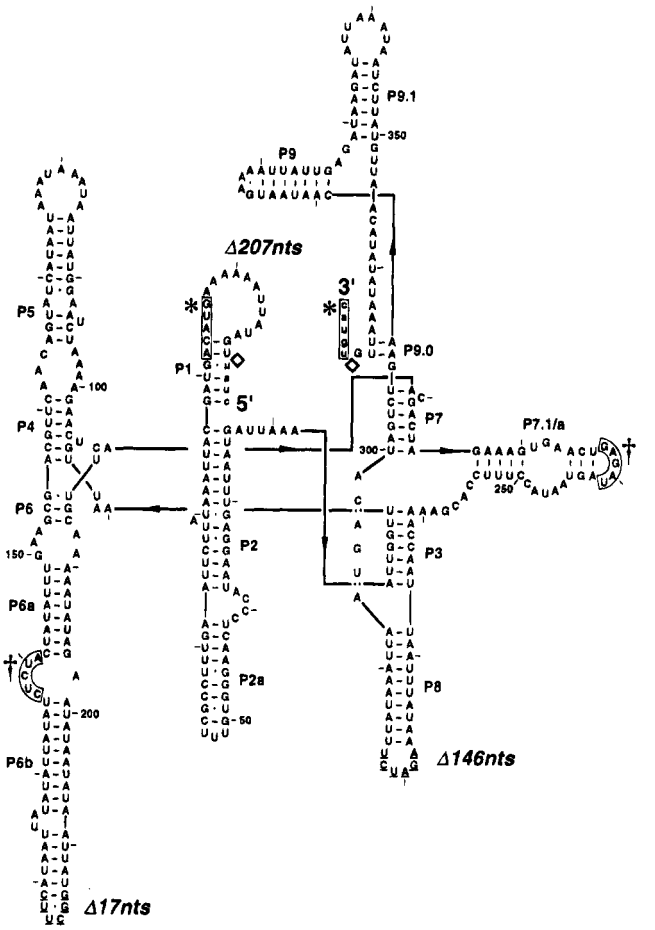

FIGURE 2: Secondary structure of the simplified bI5 splicing precursor. Splice sites are indicated by diamonds. Upper and lower case letters indicate intron and exon sequences, respectively. Sequences which form helices P10 and P11 are boxed and are indicated by an asterisk and dagger, respectively. Position and size of deletions are indicated; bases not encoded in the native sequence are underlined. The simplified intron is renumbered from 1 to 368. The entire 5′ and 3′ exons (not shown) are 35 and 55 nt, respectively.

Within error, our data require k_{II} to be at least three times faster than k_I. The ligated product is generated in ~60% yield as compared with the fraction of reactive precursor.

Our interpretation for the major off-pathway reaction is shown enclosed by the dashed line in Scheme 1. The intron−3′ exon intermediate accumulates in significant yield at early time points, as determined by reactions performed with internally labeled precursor, but it does not appear to chase into ligated exons (data not shown). Furthermore, production of free 5′e via hydrolysis at the 5′ splice site can

Scheme 1

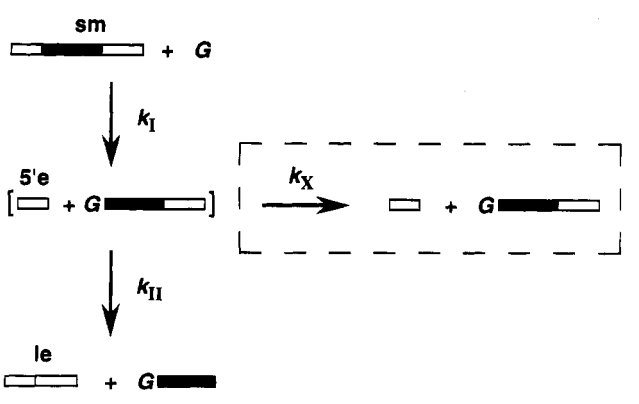

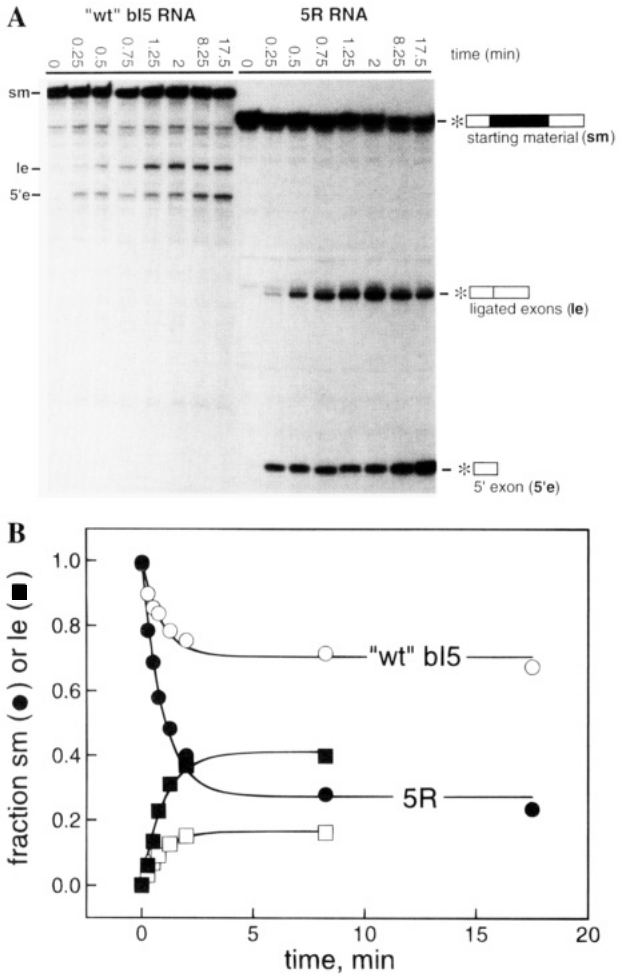

FIGURE 3: CBP2-facilitated processing of native bI5 and simplified 5R precursors in 7 mM $MgCl_2$ at pH 7.6. (A, top) Autoradiogram of splicing products of 5′-end-labeled RNA (position of label is indicated by asterisk) resolved by denaturing gel electrophoresis: sm, starting material; le, ligated exons; 5′e, 5′ exon. (B, bottom) Quantitative analysis of splicing reactions. Open and closed symbols correspond to "wt" bI5 and simplified 5R (Figure 2) precursors, respectively. Circles indicate reaction of starting material, curves are fit as described in the Experimental Procedures; squares show formation of the biologically relevant product, ligated exons, and are fit to fraction le $= f_1 e^{-k_{obs}t} - f_1$.

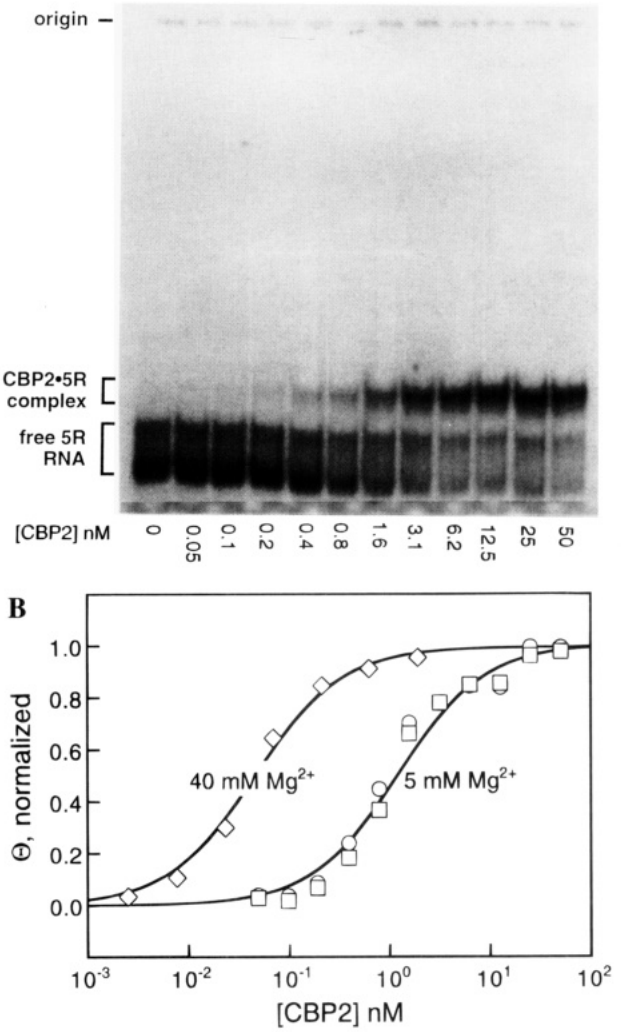

FIGURE 4: Determination of K_d^{CBP2}. (A, top) Native gel mobility shift assay of bI5•CBP2 complex formation at 5 mM $MgCl_2$. (B, bottom) Analysis of fraction bound, θ, normalized to the maximum extent of binding observed at high protein concentrations, for RNA−protein complexes formed at 5 mM (squares, analyzed by mobility shift; circles, analyzed by filter binding) and at 40 mM (diamonds, analyzed by filter binding).

be ruled out because in our protocol intron refolding and CBP2 binding require a 60 min preincubation (in the absence of pG), during which time there is essentially no observed cleavage (see the zero minute time points in Figure 3A). Thus, either the 5′ exon is lost by premature dissociation or a fraction of precursor molecules are simply incompetent for ligation (Scheme 1). At very long time points some 5′ exon is produced by apparent recleavage of the ligated exons.

The native and simplified introns react at similar rates in the initial fast phase both in protein-dependent and -independent reactions and at low (7 mM) and high (40 mM) magnesium ion concentrations (Table 1). The reactions of the bI5 and 5R precursors differ not in the observed k_{cat}, but rather in the fraction folded: a smaller fraction of the native intron is reactive as compared with the 5R intron. However, the 5R precursor retains the salient protein-dependent splicing activity of the parent molecule: at 7 mM magnesium ion, processing is accelerated ≥500-fold by CBP2 for both bI5 and 5R. Subsequent experiments are facilitated by using the smaller 5R precursor; we refer to this intron as "bI5" for simplicity.

RNA Binding by CBP2 Protein and Mg^{2+} Ion Are Coupled. Complex formation between precursor RNA and CBP2 is readily followed by a native gel mobility shift assay (Figure 4A); the CBP2•bI5 complex migrates as a well behaved and discrete complex in the gel. The equilibrium dissociation constant at 5 mM $MgCl_2$ determined by either mobility shift or filter binding is 1.0 ± 0.3 nM (squares and circles, respectively, in Figure 4B). Values obtained for apparent dissociation constants were independent of incubation time and the concentration of RNA was significantly less than the observed K_d (see Experimental Procedures for details), establishing that the complex was at equilibrium. The binding curves are well fit as a simple bimolecular process. The data are significantly less well fit by equations describing multiple binding by CBP2 (data not shown). Taken together with the velocity sedimentation data demonstrating that CBP2 is a monomer in solution (Figure 1), we adopt the simplest explanation that the splicing factor forms a 1:1 complex with the 5R precursor.

In the absence of favorable compensating interactions, magnesium ion would be expected to weaken CBP2 binding by reducing the strength of any electrostatic contribution to the protein-RNA interaction [for examples with DNA, see

Table 1: Comparison of k_{cat} and Fraction Reactive (f_1) for Native bI5 and 5R at pH 7.6 and 35 °C[a]

			bI5		5R	
[$MgCl_2$] (mM)	CBP2	species monitored[b]	k_{cat} (min^{-1})	f_1	k_{cat} (min^{-1})	f_1
7	+[c]	sm	1.1	0.30	1.1	0.73
7	+[c]	le	1.1	0.17	1.0	0.41
40	+[c]	sm	0.77	0.39	1.8	0.75
40	+[c]	le	0.65	0.29	1.5	0.58
7	−	sm	~0.002[d]		~0.002[d]	
40	−	sm	0.05	0.51	0.14	0.80
40	−	le	0.05	0.40	0.14	0.49

[a] Errors are ±20% except for slow reactions ($k_{obs} \leq 0.01$ min^{-1}), for which errors are ±50%. [b] sm, reaction of starting material; le, formation of ligated exons. [c] Doubling the CBP2 concentration from 50 to 100 nM yielded no change in rate, demonstrating that the protein was saturating. [d] Determined from initial rates after correcting for assumed endpoints of 35 and 70% for bI5 and 5R, respectively.

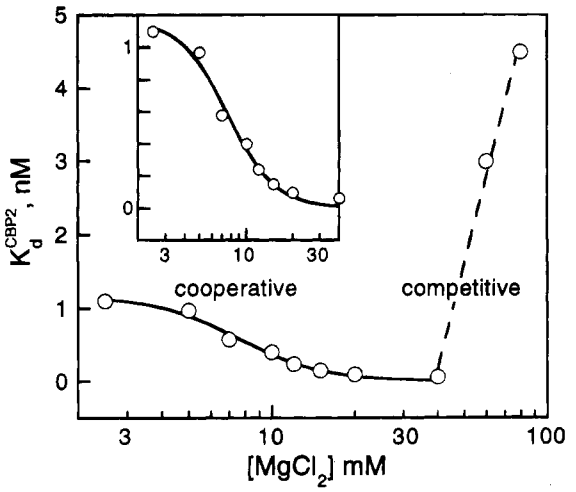

FIGURE 5: Binding by magnesium ion and CBP2 are coupled. Dissociation constants, K_d^{CBP2}, were determined by filter binding. The solid line represents a fit to a cooperative binding model, $K_d = K_{5mM}/\{1 + ([Mg^{2+}]/[Mg^{2+}]_{1/2})^n\}$ where $[Mg^{2+}]_{1/2}$ is the magnesium ion concentration at half saturation and n is the number of ions involved in the cooperative transition, and yields $n = 2.8 \pm 0.5$. [The K_d at 5 mM $MgCl_2$ was taken as the reference point because chemical accessibility experiments indicate that at this ion concentration the secondary structure is formed but there is little or no tertiary structure (data not shown)]. The dashed line does not represent a specific model for competition by magnesium ion but simply emphasizes the large competitive binding component.

Record et al. (1977) and Lohman et al. (1980)]. In striking contrast, CBP2 binding is strengthened 20-fold at 40 mM Mg^{2+} as compared with binding at 5 mM (Figure 4B, compare diamonds and circles). Above 40 mM binding becomes weaker with increasing magnesium ion: in this regime the cation behaves as a competitor (Figure 5). The magnesium-dependent folding transition is cooperative and is consistent with a transition involving approximately ~3 ions that is complete at ~40 mM magnesium (Figure 5). In light of the well established view that tertiary folding of several group I ribozymes is specifically stabilized by divalent ions (Latham & Cech, 1989; Celander & Cech, 1991; Heuer et al., 1991), tighter binding with increased magnesium ion concentrations strongly implies CBP2 is a *tertiary structure* binding protein. That is, CBP2 binds more tightly to the native higher order structure than to isolated elements of the secondary structure.

Equilibrium dissociation constants as a function of $MgCl_2$ for the CBP2 complex with native bI5, 5R, nrdB, and

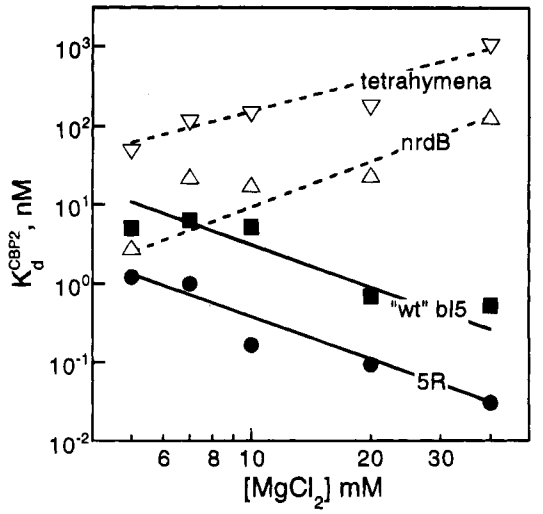

FIGURE 6: Coupled binding assay distinguishes between specific and semispecific complexation by CBP2. Dissociation constants were determined by filter binding at pH 7.6. Negative and positive slopes imply net coupling or net competition by Mg^{2+} for RNA binding by CBP2. In order to illustrate the wide range of equilibrium dissociation constants observed, K_d^{CBP2}'s are plotted on a logarithmic scale (cf. Figure 5, where dissociation constants are plotted on a linear scale).

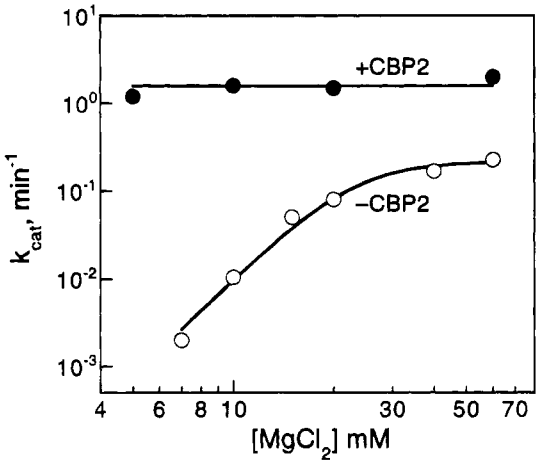

FIGURE 7: k_{cat} as a function of magnesium ion concentration for protein-facilitated and protein-independent self-splicing reactions. Reactions were performed at pH 7.6 with 2 mM pG; endpoints, ~70% reacted, were similar for all reactions. The rate of the protein-independent (-CBP2) reaction as a function of [$MgCl_2$] is fit to a cooperative (Mg^{2+}) binding model analogous to that described in Figure 5 and yields $n \approx 3-4$; the rate reaches a near plateau above 40 mM [$MgCl_2$] at $k_{cat} = 0.2$ min^{-1}.

Tetrahymena splicing precursors are compared in Figure 6. (The nrdB and *Tetrahymena* precursors are self-splicing at low Mg^{2+} ion concentrations and have no known protein facilitators.) Although the nrdB, bI5, and 5R precursors bind similarly at 5 mM $MgCl_2$, coupling with magnesium is only seen with the two versions of the bI5 intron. At 40 mM Mg^{2+} CBP2 readily discriminates against the nrdB and *Tetrahymena* introns ($K_{rel} = 10^3-10^4$, $\Delta\Delta G° = 4-6$ kcal/mol). Similar binding at low magnesium concentrations for cognate 5R and noncognate nrdB introns provides evidence for a significant less-specific component of binding by CBP2: the splicing factor may either have a strong generalized affinity for RNA or may recognize, in part, features conserved among group I introns.

Magnesium Ion Dependence of Splicing. Saturating concentrations of CBP2 render the splicing reaction es-

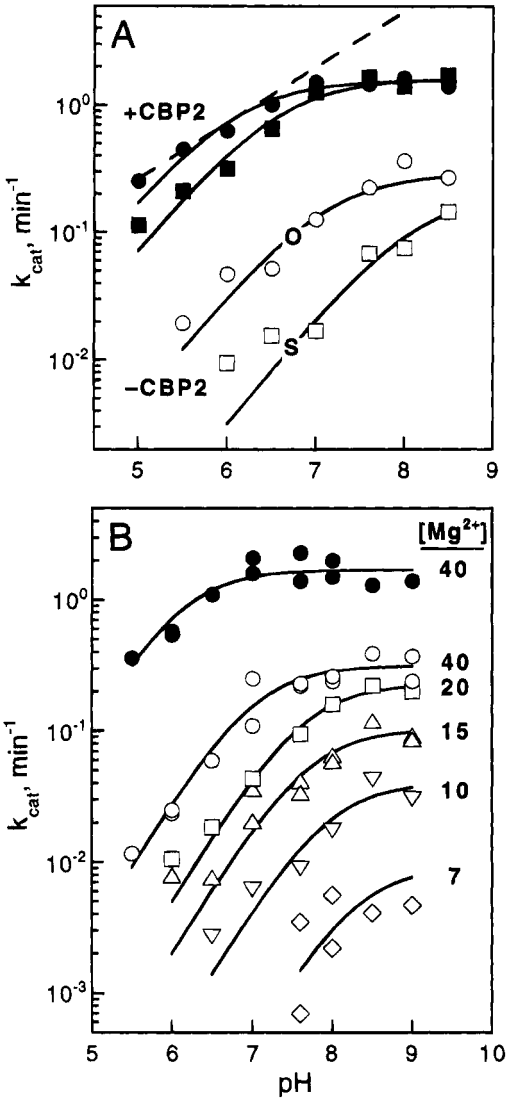

FIGURE 8: Determination of rate-limiting chemistry and conformational steps. (A) Thio effect and pH dependence for protein-facilitated (solid symbols) and -independent (open symbols) reactions for all-phosphate (circles) and $R_p(1)$ thio (squares) precursors at 40 mM $MgCl_2$ with 2 mM pG. As described in the text, both pG and CBP2 are saturating. Solid lines represent a fit to the model described by Scheme 2 which predicts that k_{cat}/pH should have a slope of 1; observed rates show a systematic deviation from this theoretical ideal. The observed slope for these reactions is 0.6. Although we cannot at present rationalize this discrepancy, nonunity slopes have been observed for both protein enzymes (Howell et al., 1986) and the hammerhead ribozyme (Dahm et al., 1993, and references therein). The dashed line extrapolates the apparent rate of chemistry for the protein-facilitated reaction to high pH. (B) pH dependence for protein-facilitated (solid symbols) and -independent (open symbols) reactions as a function of [$MgCl_2$] at 2 mM pG. For solid symbols, [CBP2] = 30 nM.

sentially insensitive to Mg^{2+}: the rate of splicing (k_{cat}) increases only 2-fold from 1.0 to 2.0 min^{-1} as the magnesium ion concentration is increased from 5 to 60 mM (Figure 7). In contrast, the rate of self-processing in the absence of protein with saturating pG increases more than 400-fold, being undetectable at 5 mM Mg^{2+} (<0.0005 min^{-1}) and plateauing at 0.2 min^{-1} at 40−60 mM magnesium ion. The dependence of k_{cat} on magnesium ion concentration has two important features. (1) Acquisition of activity in the absence of protein is cooperative and is best fit by a model in which 3−4 ions bind in a primary folding transition (Figure 7). (2) High magnesium ion concentrations (40−60 mM) alone *do not* completely substitute for protein facilitation by CBP2. The maximal rate for the protein-independent reaction is ~8-fold slower than that for the protein-facilitated reaction.

Similar Rate-Limiting Steps for Both Protein-Facilitated and Protein-Independent Reactions. For several reactions of model substrates and catalytic RNAs, phosphorothioate substitution has been shown to lower the intrinsic chemical reactivity of the phosphate diester 2−10-fold (Herschlag et al., 1991; Herschlag & Khosla, 1994; Zaug et al., 1994). An independent method to probe the chemical step is by following the pH dependence of the reaction rate. A log-linear rate dependence with pH with slope +1 provides strong evidence for a rate-limiting step involving loss of one proton in the transition state: chemistry, most generally.

A unique R_p phosphorothioate linkage at the 5′ splice site was incorporated into an RNA precursor, termed $R_p(1)$ (see Experimental Procedures). Rates of splicing in the presence and absence of CBP2 with saturating pG (k_{cat} conditions) as a function of pH for both all-phosphate and $R_p(1)$ precursors at 40 mM Mg^{2+} are illustrated in Figure 8A. At low pH, there is both a log-linear pH dependence and a thio effect [compare all-phosphate precursor (circles) and the $R_p(1)$ precursor (squares)] for both protein-facilitated and -independent reactions (Figure 8A, solid and open symbols, respectively). Doubling the concentration of CBP2 yielded no change in rate, confirming the protein was saturating for both all-phosphate and $R_p(1)$ precursors. Nor is the decrease in rate with lower pH due to the reactions becoming subsaturating with respect to guanosine, as it will be shown later (Table 2) that K_m for pG remains much less than 2 mM at low pH with or without CBP2. Moreover, we determined K_m with the $R_p(1)$ precursor at 40 mM Mg^{2+} at pH 7.6 and 5.5 to be ~30% smaller than with the all-phosphate precursor, so the concentration of pG remains saturating.

The thio effects (defined as $k_{phosphate}/k_{phosphorothioate}$) for the protein-facilitated and -independent reactions (determined by comparison of reactions performed side by side at several pH values) are 2.2 ± 0.2 and 3.8 ± 0.5, respectively. The observation of a thio effect of this magnitude provides strong evidence that the highest barrier on the reaction coordinate faced by both reactions is chemistry at pH <6.5. The thio effects for the protein-independent and protein-facilitated reactions are *not* the same within error, strongly suggesting that the transition states for the two reactions are not identical.

At higher pH (>7.5) both the thio effect disappears and k_{cat} becomes independent of pH for the protein-facilitated reaction (Figure 8A, closed symbols), strongly suggestive that a new (presumably conformational) step has become rate limiting (Scheme 2).

Scheme 2

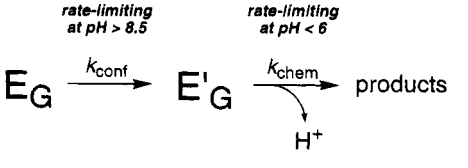

According to this model, the rate of some conformational step determines the upper limit to the rate of reaction even though the rate of the chemical step continues to increase with pH. The disappearance of the thio effect provides evidence against the other alternative, that a functional group important for chemistry with a $pK_a \approx 7$ is being titrated over this region (Herschlag & Khosla, 1994). Analogous behavior is observed for the protein-independent self-splicing reaction,

Table 2: Kinetic Parameters for GuanosineAddition by the 5R Precursor at 35 °C[a]

pH	[$MgCl_2$] (mM)	CBP2	k_{cat} (min^{-1})	k_{cat}/K_m (10^3 M^{-1} min^{-1})	K_m (μM)
7.6	7	+	1.1	7.0	120
	7	−	0.002	0.010	280
	40	+	1.6	34	60
	40	−	0.22	1.2	310
	80[b]	+	2.2		
	80[b]	−	0.32		
5.0	7	+	0.2	0.65	290
	40	+	0.26	1.0	260
5.5	40	−	0.028	0.046	420

[a] Determined from complete kinetic profiles like those shown in Figure 9. Errors are ±20% except for slow reactions ($k_{obs} \leq 0.01$ min^{-1}), for which errors are ±50%. [b] Determined from measurements at a single (saturating) pG concentration of 2 mM.

although it was not possible to follow the reaction at a pH sufficiently high to observe convergence between reaction rate for the all-phosphate and $R_p(1)$ precursors (Figure 8A, open symbols).

The pH-dependence data permit estimation of the rate of the chemical step (k_{chem}) at pH 7.6 for the protein-facilitated reaction. Extrapolation of the linear part of the curve below pH 6.5 (Figure 8A, dashed line) yields a rate of 5 ± 1 min^{-1} at pH 7.6, 3-fold faster than k_{cat} at this pH. The data for the reactions shown in Figure 8A were obtained at 40 mM magnesium ion; analogous behavior for the protein-facilitated reaction was observed at 7 mM magnesium in the presence of CBP2 (data not shown), as expected given that k_{cat} is nearly independent of magnesium ion concentration for the protein-facilitated reaction (Figure 7).

The pH dependences of reactions at decreased magnesium ion concentrations show kinetic behavior analogous with that at 40 mM magnesium ion (Figure 8B). At pH ≤7, all protein-independent reactions show a log-linear dependence of rate on pH, consistent with rate-limiting chemistry. At higher pH, the rate of reaction is pH independent, consistent with a rate-limiting conformational step (Scheme 2).

With decreasing magnesium ion concentrations, the pH profiles (Figure 8B) shift both downward and to the right (the inflection point or apparent pK_a occurs at higher pH). The downward shift with decreasing magnesium ion concentrations reports the decrease in fraction of folded intron. The same process is monitored as CBP2 binding strength and k_{cat} determined as a function of magnesium ion concentration (Figures 5 and 7, respectively). However, slowed self-splicing due to a decrease in the fraction of active molecules would not by itself change the apparent pK_a. The shift in apparent pK_a to higher pH with decreasing magnesium ion concentrations, or for the protein-independent reaction as compared with the protein-facilitated one, is most simply explained by the decrease in the rate of chemistry being larger than the decrease in the maximum rate (limited by the conformational change). For slowed chemistry, the log-linear rate dependence is maintained until higher pH before it overtakes the rate of the conformational step. This conclusion is corroborated by the observation discussed in the previous section that the thio effect is different for the protein-facilitated and -independent reactions, consistent with differences in the transition states for these two reactions.

Kinetic Constants. Kinetic parameters were determined by following complete rate profiles as a function of pG concentration as shown for the protein-facilitated reaction at 7 mM Mg^{2+} in Figure 9. These data give k_{cat} = 1.0 min^{-1} and K_m = 120 μM. The second-order rate constant for reaction of free nucleophile with the precursor, k_{cat}/K_m = 7 × 10^3 $M^{-1}min^{-1}$, was determined from the slope of the rate dependence at low pG (inset in Figure 9B) and was therefore determined independently of the values of k_{cat} and K_m.

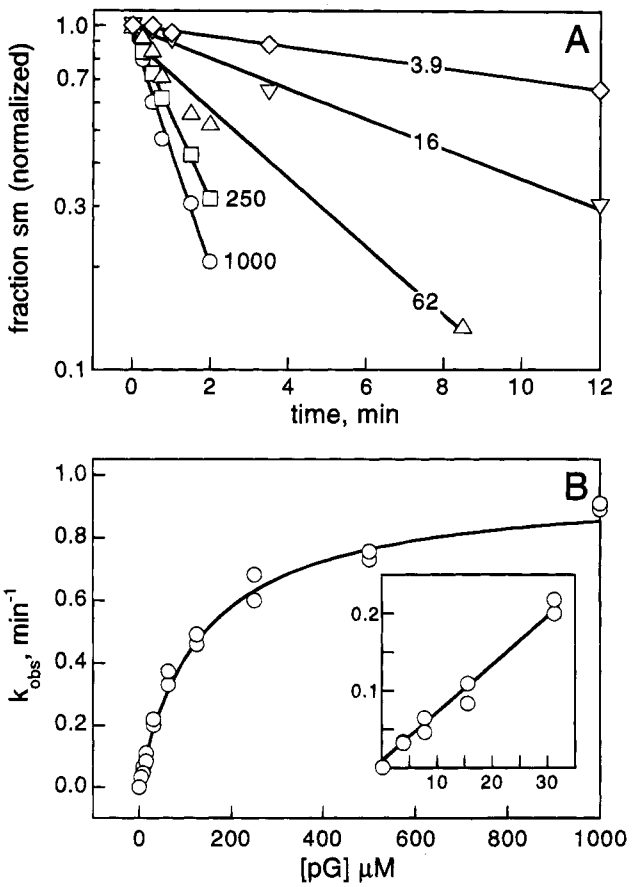

FIGURE 9: Determination of Michaelis parameters for the protein-facilitated reaction at 7 mM $MgCl_2$ and pH 7.6. (A) Determination of first-order rates as a function of [pG] (values given in μM). (B) Rate data are fit to the Michaelis–Menton equation: $k_{obs} = k_{cat}[pG]/\{K_m + [pG]\}$. (Inset) Data at low pG concentrations; the slope of the line yields k_{cat}/K_m.

A superficial comparison of the K_m values in Table 2 might suggest that CBP2 causes tighter binding of pG (e.g., K_m decreases from 280 to 120 or from 310 to 60 μM upon CBP2 binding at 7 and 40 mM Mg^{2+} ion, respectively). However, K_m is *not* equal to the dissociation constant for pG, K_d^{pG}, at pH 7.6 for the protein-facilitated reaction. Inspection of Figure 8A indicates that K_m reflects a change in rate-limiting step from chemistry at low pG concentration (at low enough concentration a step involving pG must become rate limiting) to the conformational change discussed in the previous section at high concentration. $k_{cat}/K_m \approx 10^4$ M^{-1} min^{-1} provides a lower limit for any second-order rate for the forward reaction and is much less than expected association rates of 10^7–10^8 M^{-1} min^{-1} for small ligand binding (Fersht, 1985). Therefore, the other major possibility, that substrate association is rate limiting under these conditions, is unlikely. Measurements of rates at pH 5.0 slows chemistry such that this step is rate limiting over the entire range of pG concentrations (Figure 8A) and is expected to yield $K_m = K_d$. Under these conditions K_m = 290 μM (Table 2). Similar arguments hold for the protein-facilitated reaction at high (40 mM) magnesium where K_m = 260 μM (see Table 2).

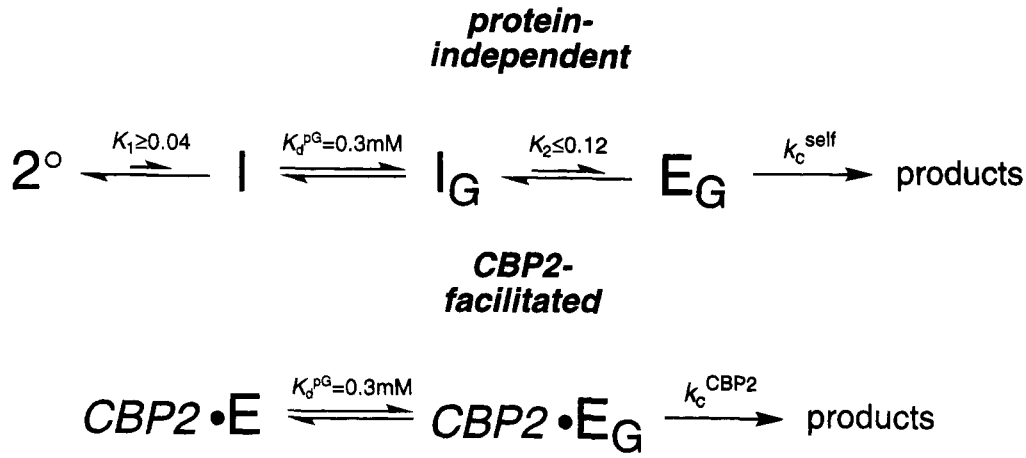

FIGURE 10: Kinetic frameworks for protein-independent and protein-facilitated self-processing reactions at 7 mM Mg^{2+}. 2°, I, and E represent secondary structure, intermediate, and active enzyme conformations of the self-processing precursor. k_c is the rate of conversion of the E_G complex and is limited by either chemistry or a conformational step as shown in Scheme 2. At pH 7.6, the self-processing reaction is limited by chemistry, whereas the CBP2-facilitated reaction is limited by a conformational step.

Two lines of evidence suggest K_m is approximately equal to K_d^{pG} at pH 7.6 for the protein-independent reaction. (1) Inspection of Figure 8A shows that chemistry is still largely rate limiting at pH 7.6 at any magnesium ion concentration, suggesting there is no change in rate-limiting step and that K_m could be equal to K_d^{pG}. (2) k_{cat} at 40 mM magnesium ion decreases 8-fold upon lowering the pH from 7.6 to 5.5, while K_m decreases by less than a factor of 2 (Table 2). This provides evidence that the rate of chemistry is much slower than dissociation of the nucleophile (McConnell et al., 1993) and supports assignment of $K_m = K_d^{pG}$ for the protein-independent reaction.

Thus, $K_d^{pG} \approx 0.3$ mM is the same, within error, for both the protein-facilitated and self-splicing reactions. Although we cannot rule out modest coupling, the data support independent binding of CBP2 and pG to the RNA.

DISCUSSION

An Experimentally Tractable Model for CBP2 Facilitation of bI5 Splicing. Overexpression of recombinant CBP2 provides abundant and pure protein for investigation of splicing *in vitro*. Deletion of nonessential regions of the RNA precursor facilitates detailed binding and mechanistic studies. Demonstration of complex formation by the mobility shift assay (Figure 4A) was not possible previously because the much larger native bI5 precursor could not be resolved from the bI5•CBP2 complex. In addition, the fraction of the native precursor that is reactive in the fast phase (~30%) is unacceptably small for careful kinetic study and, for example, would have made intractable the diagnostic phosphorothioate and pH-dependence experiments used to disentangle the rate-limiting chemical and conformational steps (Figure 8A).

We find that CBP2 is a monomer is solution and forms a discrete, well behaved complex with the simplified 5R precursor RNA as visualized in a native gel mobility shift assay. RNA binding by CBP2 and Mg^{2+} are coupled, strongly implying that CBP2 recognizes the catalytically active three-dimensional intron tertiary structure. The coupled binding assay (Figure 6) permits dissection of generalized nonspecific and specific binding by CBP2. We note that CBP2 would bind extremely tightly to a hypothetical intron that displayed features required for interaction with CBP2 and whose relevant three-dimensional structure was already folded at low magnesium ion concentrations ($K_d \ll$ 60 pM, the observed K_d at 40 mM Mg^{2+}, Figure 5).

Efficient Protein-Dependent Splicing. The bI5•CBP2 complex performs the splicing reaction as efficiently as any known group I intron with a k_{cat}/K_m of $7-30 \times 10^3$ M^{-1} min^{-1} and k_{cat} of $1-2$ min^{-1}. These two kinetic parameters reflect chemistry and a putative conformational step, respectively. With respect to k_{cat}/K_m, which represents a lower limit on any second-order rate constant, we argue that binding of pG must be fast. pG binding to bI5 is characterized by an equilibrium dissociation constant of 0.3 mM and within error is not coupled with CBP2 binding. The formation of ligated exons occurs at the same rate as reaction of the precursor with guanosine (Table 1); thus, a step up to or including the first transesterification reaction is rate limiting for the overall reaction.

Since the rate of the protein-facilitated reaction is largely independent of magnesium ion concentration, while the rate of the protein-independent self-processing reaction decreases sharply with decreasing Mg^{2+} concentrations (Figure 7), the fold enhancement achieved via facilitation by CBP2 can be made (nearly) arbitrarily large. At 7 mM magnesium, CBP2 accelerates splicing 500-fold (Table 2); at 5 mM magnesium the rate acceleration is estimated to be $\geq$2000-fold.

Kinetic Framework. The contributions that CBP2 binding makes to splicing by bI5 are summarized in the kinetic framework shown in Figure 10. The following is a justification for the individual steps, proceeding from right to left.

Phosphorothioate substitution and pH-dependence experiments reveal that at 7 mM Mg^{2+} the actual chemical step (attack by guanosine nucleophile) is rate limiting for the protein-facilitated reaction below pH 6 and for self-processing below pH 8.5. Reaction is limited by a conformational step for both reactions at higher pH. Strikingly, in the physiological pH range (7−7.5), the chemical step is rate limiting for self-splicing, whereas protein facilitation of splicing causes a change in rate-limiting step such that a conformational step now becomes rate limiting (Figure 8A,B). An open question is what contribution a rate-limiting conformational change might make to the splicing reaction.

We have no evidence for additional steps or intermediates in the CBP2-facilitated splicing reaction. Thus, our proposed mechanism for reaction of the CBP2•bI5 complex is adequately represented by two kinetically significant steps: pG

Table 3: Comparison of Guanosine Addition and Net Exon Ligation Rates for Group I Introns

precursor	k_{cat}/K_m (10^3 M^{-1} min^{-1})	k(formation of le)[a] (min^{-1})	rate limiting step	K_d^{pG} (mM)
bI5•CBP2 complex[b]	7.0	1.0	1st	0.3
LSU•CYT18 complex[c]		0.15	1st[d]	
Tetrahymena LSU[e]	28	0.9	1st[d]	0.09[f]
Anabaena $tRNA^{Ile}$[g]	46	0.3	2nd[h]	0.24

[a] Reactions performed with (near) saturating guanosine, pG or GTP nucleophile. [b] 52 mM Hepes (pH 7.6), 50 mM KCl, 20 mM NaCl, 7 mM $MgCl_2$, 35 °C; pG nucleophile. [c] 25 mM Tris (pH 7.5), 5 mM $MgCl_2$, 100 mM KCl, 37 °C; GTP nucleophile (Saldanha *et al.*, 1995). [d] Although not stated by the original authors, the first step appears to be rate limiting for the overall reaction because there is little observed buildup of the splicing intermediate, guanosine−intron−3′ exon. [e] 30 mM Tris (pH 7.5), 5 mM $MgCl_2$, 100 mM $(NH_4)_2SO_4$, 30 °C; guanosine nucleophile (Bass & Cech, 1986). [f] Determined with ribozyme construct; pG nucleophile (McConnell *et al.*, 1993). [g] 25 mM Hepes (pH 7.5), 15 mM $MgCl_2$, 32 °C; guanosine nucleophile (Zaug *et al.*, 1993). [h] The first step of splicing for the *Anabaena* precursor occurs with k_{cat} = 12 min^{-1}.

binding and conversion of the ternary complex (Figure 10).

At (near) saturating magnesium ion concentrations, the rate of the protein-independent reaction is ~8-fold slower than for reaction by the bI5•CBP2 complex. This difference in rates could in principle report a slowed rate-limiting chemical/conformational step. Footprinting and quantitative cross-linking experiments (K.M.W. and T.R.C., manuscript in preparation) indicate the difference in rates reflects instead a partially folded structural intermediate, suggesting the difference is due to an additional conformational equilibrium. Thus, the protein-independent reaction must overcome an additional barrier as compared to the protein-facilitated reaction. This barrier is shown as the I(intermediate) → E(active enzyme) transition in Figure 10.

Evidence for a magnesium-facilitated folding transition over the range 5−40 mM Mg^{2+} is provided by both the observed positive coupling between magnesium ion and CBP2 binding (Figure 5) and by the increase in k_{cat} with magnesium ion concentration. This folding process involves cooperative binding of ~3 additional magnesium ions (as compared with the structure at 5 mM) and is shown as the 2° (secondary structure formed) → I transition in Figure 10. The assignment of the precursor to a state in which only the secondary structure is formed at 7 mM $MgCl_2$ is supported by chemical footprinting studies (Gampel & Cech, 1991). In contrast, footprinting with Fe(II) reveals little protection of the phosphoribose backbone, suggestive of little or no tertiary folding (K.M.W. and T.R.C., manuscript in preparation).

In sum, self-processing of the bI5 intron is estimated to be 3 orders of magnitude slower than the rate of CBP2-facilitated splicing at physiological pH (7−7.5) and 5 mM Mg^{2+}. Slow self-processing principally reports the fact that the RNA is in an active conformation only a small fraction of the time.

Comparison with Other RNA-Catalyzed Reactions. The CBP2•bI5 complex splices as well as other well characterized group I introns. k_{cat} for the guanosine-*Tetrahymena* precursor complex is 0.9 min^{-1} (Bass & Cech, 1986), essentially identical to that reported here for bI5 (Table 3). The *Anabaena* intron undergoes the first step with a rate of 12 min^{-1}; however, the rate for formation of ligated exons, ~0.3 min^{-1} (Zaug et al., 1993), is actually somewhat slower than the net rate of exon ligation for bI5. The CYT18 protein, a mitochondrial tyrosyl-tRNA synthetase, facilitates splicing for diverse group I introns in *Neurospora* including the LSU intron; k_{cat} for this complex is 0.15 min^{-1} (Saldanha et al., 1995), 7-fold slower than that observed here (Table 3).

Both k_{cat}/K_m and the dissociation constant for the guanosine nucleophile, $K_d^{(p)G}$, are the same within factors of 6 and 3, respectively, for splicing of the bI5•CBP2 complex and of the *Tetrahymena* and *Anabaena* precursors (Table 3). k_{cat}/K_m is thought to reflect the chemical step for all three introns (see Results; Legault et al., 1992; Zaug et al., 1993). Moreover, ribozyme derivatives of both the *Tetrahymena* and *Anabaena* introns and the intact bI5 precursor exhibit a change in rate-limiting step from chemistry to a conformational step in the physiological pH range (Herschlag & Khosla, 1994; Zaug et al., 1994). The present data demonstrate a similar rate-limiting conformational step for both protein-independent and protein-facilitated group I splicing reactions in the context of an intact precursor. Taken together, these data suggest that fundamental strategies for transition state stabilization, nucleophile binding and progression along the reaction coordinate are broadly conserved among group I introns, whether acting as self-splicing RNAs or as protein−RNA complexes. These features are faithfully recapitulated by intron-derived ribozymes.

Our kinetic framework (Figure 10) suggests several comparisons with other simple protein-facilitated RNA-catalyzed reactions including CYT18 facilitation of group I intron splicing and the contribution made by the C5 protein to tRNA processing by the RNase P holoenzyme. High magnesium ion concentrations do not detectably promote splicing of the *Neurospora* LSU intron (Atkins & Lambowitz, 1987); however, CYT18 does facilitate splicing by mutants of the heterologous phage T4 td intron that self-splice at high but not low [$MgCl_2$] (Mohr et al., 1992). The C5 protein accelerates k_{cat} of the RNase P holoenzyme 20-fold over that observed for the RNA alone reaction under optimized conditions in high salt (Reich et al., 1988). Thus, like bI5, a recurrent theme is that magnesium ion does not compensate completely for specific protein facilitation in these systems. Moreover, like bI5, acquisition of both structure and catalytic activity (monitored by cross-linking and k_{cat}/K_m, respectively) for RNase P RNA is coupled with Mg^{2+} binding (Smith & Pace, 1993). Footprinting experiments indicate that both CYT18 (Mohr et al., 1994) and C5 (Talbot & Altman, 1994) bind to RNA elements widely separated in the secondary structure, implying that, like CBP2, these proteins recognize the folded three-dimensional structure of their cognate RNAs. Thus, the three proteins (CBP2, CYT18, and C5) may share several strategies for facilitating RNA catalysis.

Implications. The framework presented in Figure 10 emphasizes the pleiotropic effects of CBP2 binding on bI5 splicing. One hypothesis commonly invoked to explain protein facilitation of RNA catalysis is that the protein cofactor promotes activity by "stabilizing the catalytically active structure of the RNA." While this statement also pertains to CBP2, it has been possible to separate several distinct contributions of protein binding to the splicing reaction. CBP2 binding energy is used to facilitate the folding reaction at two defined stages and to accelerate the rate of the chemical step in the folded molecule. The kinetic model presented here provides a framework within which to analyze and interpret the effects of mutation, nucleophile

binding, ionic environment, and protein facilitation on RNA processing. Principles derived from investigation of this simple protein-facilitated but intrinsically RNA-catalyzed reaction will likely provide mechanistic guidelines applicable to more complex cellular RNA−protein machines.

ACKNOWLEDGMENT

We thank A. Gooding and C. Grosshans for oligonucleotide synthesis and T. McConnell and P. Bevilacqua for helpful discussion.

REFERENCES

Atkins, R. A., & Lambowitz, A. M. (1987) *Cell 50*, 331−345.
Bass, B. L., & Cech, T. R. (1984) *Nature 308*, 820−826.
Bass, B. L., & Cech, T. R. (1986) *Biochemistry 25*, 4473−4477.
Brehm, S. L., & Cech, T. R. (1983) *Biochemistry 22*, 2390−2397.
Cech, T. R. (1990) *Annu. Rev. Biochem. 59*, 543−568.
Celander, D. W., & Cech, T. R. (1991) *Science 251*, 401−407.
Coetzee, T., Herschlag, D., & Belfort, M. (1994) *Genes Dev. 8*, 1575−1588.
Dahm, S. C., Derrick, W. B., & Uhlenbeck, O. C. (1993) *Biochemistry 32*, 13040−13045.
Fersht, A. (1985) *Enzyme Structure and Mechanism*, 2nd ed., pp 150−151, W. H. Freeman and Co., New York.
Gampel, A., & Tzagoloff, A. (1987) *Mol. Cell. Biol. 7*, 2545−2551.
Gampel, A., & Cech, T. R. (1991) *Genes Dev. 5*, 1870−1880.
Gampel, A., Nishikimi, M., & Tzagoloff, A. (1989) *Mol. Cell. Biol. 9*, 5424−5433.
Garriga, G., & Lambowitz, A. M. (1984) *Cell 38*, 631−641.
Gill, S. C., & von Hippel, P. H. (1989) *Anal. Biochem. 182*, 319.
Guo, Q., & Lambowitz, A. M. (1992) *Genes Dev. 6*, 1357−1372.
Herschlag, D., & Khosla, M. (1994) *Biochemistry 33*, 5291−5297.
Herschlag, D., Piccirilli, J. A., & Cech, T. R. (1991) *Biochemistry 30*, 4844−4854.
Heuer, T. S., Chandry, P. S., Belfort, M., Celander, D. W., & Cech, T. R. (1991) *Proc. Natl. Acad. Sci. U.S.A. 88*, 11105−11109.
Hicke, B. J., Christian, E. L., & Yarus, M. (1989) *EMBO J. 8*, 3843−3851.
Howell, E. E., Villafranca, J. E., Warren, M. S., Oatley, S. J., & Kraut, J. (1986) *Science 231*, 1123−1128.
Jaeger, L., Westhof, E., & Michel, F. (1991) *J. Mol. Biol. 221*, 1153−1164.
Kunkel, T. A. (1985) *Proc. Natl. Acad. Sci. U.S.A. 82*, 488−492.
Lambowitz, A. M., & Perlman, P. S. (1990) *Trends Biochem. Sci. 15*, 440−444.
Latham, J. A., & Cech, T. R. (1989) *Science 245*, 276−282.
Legault, P., Herschlag, D., Celander, D. W., & Cech, T. R. (1992) *Nucleic Acids Res. 20*, 6613−6619.
Lohman, T. M., deHaseth, P. L., & Record, M. T., Jr. (1980) *Biochemistry 19*, 3522−3530.
McConnell, T. S., Cech, T. R., & Herschlag, D. (1993) *Proc. Natl. Acad. Sci. U.S.A. 90*, 8362−8366.
McGraw, P., & Tzagoloff, A. (1983) *J. Biol. Chem. 258*, 9459−9468.
Michel, F., Hanna, M., Green, R., Bartel, D. P., & Szostak, J. W. (1989) *Nature 342*, 391−395.
Mohr, G., Zhang, A., Gianelos, J. A., Belfort, M., & Lambowitz, A. M. (1992) *Cell 69*, 483−494.
Mohr, G., Caprara, M. G., Guo, Q., & Lambowitz, A. M. (1994) *Nature 370*, 147−150.
Moore, M. J., & Sharp, P. A. (1992) *Science 256*, 992−997.
Noller, H. F., Hoffarth, V., & Zimniak, L. (1992) *Science 256*, 1416−1419.
Partono, S., & Lewin, A. S. (1988) *Mol. Cell. Biol. 8*, 2562−2571.
Partono, S., & Lewin, A. S. (1990) *Proc. Natl. Acad. Sci. U.S.A. 87*, 8192−8196.
Partono, S., & Lewin, A. S. (1991) *Nucleic Acids Res. 19*, 605−609.
Rajagopal, J., Doudna, J. A., & Szostak, J. W. (1989) *Science 244*, 692−694.
Record, M. T., Jr., deHaseth, P. L., & Lohman, T. M. (1977) *Biochemistry 16*, 4791−4796.
Reich, C., Olsen, G. J., Pace, B., & Pace, N. R. (1988) *Science 239*, 178−181.
Saldanha, R. J., Patel, S. S., Surendran, R., Lee, J. C., & Lambowitz, A. M. (1995) *Biochemistry 34*, 1275−1287.
Slim, G., & Gait, M. J. (1991) *Nucleic Acids Res. 19*, 1183−1188.
Smith, D., & Pace, N. R. (1993) *Biochemistry 32*, 5273−5281.
Squires, C. H., Childs, J., Eisenberg, S. P., Polverini, P. J., & Sommer, A. (1988) *J. Biol. Chem. 263*, 16297−16302.
Talbot, S. J., & Altman, S. (1994) *Biochemistry 33*, 1399−1405.
van der Horst, G., & Tabak, H. F. (1985) *Cell 40*, 759−766.
Wong, I., & Lohman, T. M. (1993) *Proc. Natl. Acad. Sci U.S.A. 90*, 5428−5432.
Zaug, A. J., McEvoy, M. M., & Cech, T. R. (1993) *Biochemistry 32*, 7946−7953.
Zaug, A. J., Davila-Aponte, J., & Cech, T. R. (1994) *Biochemistry 33*, 14935−14947.

BI9502304